Interaction of a Baroclinic Vortex with Background Shear: Application to Hurricane Movement

CHUN-CHIEH WU AND KERRY A. EMANUEL

Center for Meteorology and Physical Oceanography, Massachusetts Institute of Technology, Cambridge, Massachusetts

(Manuscript received 6 September 1991, in final form 27 February 1992)

ABSTRACT

Most extant studies of tropical cyclone movement consider a barotropic vortex on a β plane. However, observations have shown that real tropical cyclones are strongly baroclinic, with broad anticyclones aloft. Also, the distribution of the large-scale potential vorticity gradient in the tropical atmosphere is very nonuniform. These properties may substantially influence the movement of such storms.

Note that the anticyclone above a hurricane will interact with the lower hurricane vortex and induce storm motion. Such interaction can be caused by both the direct effect of ambient vertical shear and the effect of vertical variation of the background potential vorticity gradient. In this paper, an attempt to isolate the effect of background vertical shear is made. The hurricane is represented in a two-layer quasigeostrophic model as a point source of mass and zero potential vorticity air in the upper layer, collocated with a point cyclone in the lower layer. The model is integrated by the method of contour dynamics and contour surgery.

The results show that Northern Hemisphere tropical cyclones should have a component of drift relative to the mean flow in a direction to the left of the background vertical shear. The effect of weak shear is also found to be at least as strong as the β effect, and the effect is maximized by a certain optimal ambient shear. The behavior of the model is sensitive to the thickness ratio of the two layers and is less sensitive to the ratio of the vortices' horizontal scale to the radius of deformation. Storms with stronger negative potential vorticity anomalies tend to exhibit more vortex drift.

1. Introduction

Studies of tropical cyclone motion have focused mainly on steering by the mean flow and the effect of background potential vorticity gradients, that is, the evolution of barotropic vortices in a barotropic flow. These effects, taken together, suggest that tropical cyclones should follow the mean large-scale (steering) flow, but with a westward and poleward relative drift.

Real tropical cyclones are strongly baroclinic, consisting of cyclones surmounted by anticyclones. The upper anticyclone, though weak in terms of wind velocity, can be very extensive. Slight displacements of the upper region of anticyclonic flow from the low-level cyclone can conceivably lead to large mutual propagation effects. Moreover, the background potential vorticity gradient may act on these two flows in very different ways.

Our present purpose is to explore the effect of background vertical shear on tropical cyclone motion. Specifically, we shall show that in the absence of background PV gradients, Northern (Southern) Hemisphere (hereafter NH and SH) tropical cyclones should drift relative to the mean flow in a direction to the left (right) of the background vertical shear because of the flow induced by the upper anticyclone, which is displaced downshear from the center of the surface cyclone. To explore the problem in a simple way, we employ a two-layer quasigeostrophic model, applying the method of contour dynamics and contour surgery.

In section 2, our present understanding of tropical cyclone motion is reviewed, and the specific questions we wish to address are identified. The model is described in section 3. The results are shown in section 4, and a summary appears in section 5.

2. Background and review

a. Review of general theories of tropical cyclone motion

The dynamics of tropical cyclone motion are complex. As pointed out by Holland (1984), a complete description would require at least a detailed knowledge of the interactions between the cyclone circulation, the environmental wind field, the underlying surface, and the distribution of moist convection. It has generally been proposed, however, that tropical cyclone motion is governed by the tropospheric average steering flow and a drift due to the presence of a background potential vorticity gradient.

The steering concept is based on the assumption that tropical cyclones are barotropic vortices embedded in

Corresponding author address: Chun-Chieh Wu, Massachusetts Institute of Technology, Center for Meteorology and Physical Oceanography, Cambridge, MA 02139.

an environmental flow and should thus move with the so-called "steering" flow, generally taken to be a weighted vertical average of the flow in the troposphere. This concept has been supported by composite observational studies by both George and Gray (1976) and Chan and Gray (1982), though a systematic directional deviation between the steering stream and storm motion was generally found. Chan and Gray suggested that this consistent deviation is caused by some other factor or factors besides the steering flow; however, there is no unique way to determine the steering flow. Chan and Gray found that the midtropospheric (500–700 mb) 5°–7° latitude radius average wind has the best correlation with the cyclone motion. Dong and Neumann (1986) also showed that there is considerable uncertainty about which layer or level determines the steering flow. A case study of Hurricane Josephine by Franklin (1990) further pointed out that in an environment with a mean vertical shear, the inappropriate initialization of the mean steering flow would result in serious errors in the barotropic storm track forecast.

Barotropic numerical studies of the evolution of hurricane-like vortices on the beta plane by Anthes and Hoke (1975), Holland (1983), DeMaria (1985), and Chan and Williams (1987) have all shown that variations of the Coriolis parameter and environmental vorticity across the tropical cyclone tend to induce a westward and poleward movement of tropical cyclones. In particular, Chan and Williams argued that the main role of the linear β term is to induce a wavenumber 1 asymmetric circulation in the initially symmetric vortex, causing the storm to be advected by the induced asymmetric flow. More recent modeling works by Fiorino and Elsberry (1989), Shapiro and Ooyama (1990), and Smith et al. (1990) also showed similar storm drifts. Fiorino and Elsberry pointed out that the nonlinear term in the vorticity equation plays an important role in orienting the asymmetric gyres and modifying the direction of hurricane movement. Most research to date assumes that barotropic drift due to the background potential vorticity gradient is the main mechanism that accounts for the deflection of tropical cyclone movement from the steering flow.

Recently, Carr and Elsberry (1990) performed a composite data analysis (using the same data as in Chan and Gray) to show evidence of drift relative to the environmental steering, which is defined as the tropospheric (surface–300 mb) 5°–7° latitude radius average wind. They found that most of the NH cyclones propagate in a particular direction with components parallel and to the left of the large-scale absolute vorticity gradient. The observational study by Franklin (1990) and numerical calculation by Evans et al. (1991) also supported this result. However, a recent numerical study by Ulrich and Smith (1991) showed that there is no definite correlation between the vortex motion and its basic-state absolute vorticity gradient. Better data from a recent field experiment in the west Pacific in 1990 (see Elsberry et al. 1990) may be helpful in understanding this problem.

b. The nonuniform distribution of potential vorticity in the troposphere

It is observed (Davis, personal communication) that the typical north–south isentropic gradient of potential vorticity (PV) in the middle-latitude troposphere during winter is much less than that associated with the planetary vorticity gradient (Fig. 1). In addition, the horizontal gradient of potential vorticity is concentrated near the tropopause (Nielsen et al. 1991).

As a preliminary effort to discover whether this is also true in the tropical troposphere, we calculate potential vorticity as $Q = -g(f + \zeta_\theta)/(\partial p/\partial\theta)$ from twice-daily National Meteorological Center Northern Hemisphere final analyses gridded datasets (on a 2.5° × 2.5° latitude–longitude grid). By interpolating the wind and pressure onto isentropic surfaces, Q is computed from a centered finite-difference scheme. The potential vorticity distributions from 5° to 60°N on the 315, 335, and 355 K isentropic surfaces at 1200 UTC 18 August 1992 [when the center of Hurricane Bob (hereafter, Bob) was located about 170 miles to the east-southeast of Charleston, South Carolina] are shown in Figs. 2a,

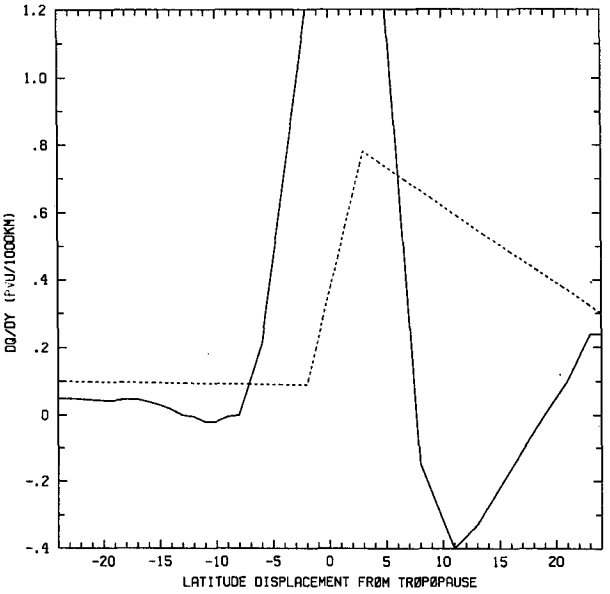

FIG. 1. The 300 K mean Northern Hemispheric north–south gradient of Ertel's potential vorticity as a function of degrees latitude north from the tropopause, for winter 1978/79. The average was performed relative to the southernmost occurrence of the 1.5-PVU (potential vorticity unit, 10^{-6} m^2 s^{-1} K kg^{-1}) contour at each latitude (5° increments) for each analysis time. The dashed line corresponds to the gradient obtained by setting the vorticity equal to the planetary vorticity and the lapse rate equal to 0.05 K mb^{-1} in the troposphere and 0.5 K mb^{-1} in the stratosphere. The observed gradient (solid line) is less than half the "planetary gradient" (dashed line) between 8° and 24° south of the tropopause (Davis, personal communication).

b, and c, respectively. Figure 2d shows the "tropopause map," which indicates the distribution of potential temperature on the 1.5 PVU (potential vorticity unit, 10^{-6} m^2 s^{-1} K Kg^{-1}) potential vorticity surface (see Davis and Emanuel 1991; Nielsen et al. 1991). Similar to Bretherton's (1966) view, the tropopause potential temperature map serves as a concise way to view the dynamic information in the upper troposphere in the absence of appreciable interior potential vorticity gradients.

On the 315 K surface (Fig. 2a), it is found that the PV distribution is quite uniform everywhere in the subtropical and tropical region. Bob appears as a local PV maximum with a PV value of 0.8 PVU. The PV gradient is mainly concentrated in eastern Canada, where the tropopause intersects this isentropic surface. On the 335 K surface (Fig. 2b), more PV contours appear in the subtropics; however, the horizontal PV gradient is most distinct along the tropopause, which extends farther south into the United States. The high PV air associated with Bob still exists at this level, but this will change dramatically as we go to higher levels. On the 355 K surface (Fig. 2c), the high potential vorticity tongue dips down to the Gulf of Mexico, acting as an intrusion of the stratospheric "reservoir" of high PV air. A negative PV anomaly shows up at the top of Bob, with a tail extending toward the downshear side. The horizontal gradient of potential vorticity in the subtropics and tropics at this level is much higher than that in the lower and middle troposphere. Figure 2d shows similar patterns as those in Fig. 2c. The lens of low PV air at the top of Bob appears as a positive potential temperature anomaly on the "dynamic tropopause." These findings cast some doubt on the applicability of the traditional theory, which relates hurricane motion to the drift of barotropic vortices embedded in a uniform background potential vorticity gradient.

Real hurricanes are characterized by anticyclonic flow near the tropopause. Since the flow typically interacts with a potential vorticity gradient that is as strong as or stronger than the gradients in the mid- or lower troposphere, it is not clear which component of the circulation has the dominant effect on the PV distribution. It is conceivable that the principal effect on tropical cyclone motion is that associated with the anticyclonic outflow near the tropopause; this effect tends to move the upper anticyclone westward and equatorward.

c. *The effect of vertical shear of the background flow*

As noted above, hurricanes have anticyclonic circulation near the tropopause, except perhaps near their centers. The reason for this can be interpreted from the potential vorticity perspective. As discussed by Hoskins et al. (1985), in the absence of diabatic heating and friction at the boundary, the mass-weighted volume integral of potential vorticity over a suitably defined domain is conserved. In other words, interior diabatic heating cannot change the mass-integrated total potential vorticity around the tropical cyclone. It only plays a role in redistributing the total potential vorticity by potential vorticity generation in the lower troposphere and potential vorticity destruction in the upper troposphere. However, because surface friction acts to destroy potential vorticity, the total potential vorticity, integrated in a volume bounded by a surface around which there is a cyclonic circulation at the sea surface, should decrease with time. From this point of view, it is expected that a region of low potential vorticity is generated in the upper troposphere above a tropical cyclone. This low PV lens near the tropopause is clearly seen in the numerical simulations of Rotunno and Emanuel (1987) and also from Figs. 2c,d in this paper. Hence, in terms of potential vorticity, a "steady-state" mature hurricane can be viewed as a diabatically and frictionally maintained constant positive potential vorticity anomaly in the lower troposphere, with an expanding negative potential vorticity anomaly in the upper troposphere.

Using the concepts of vortex interaction, a baroclinic tropical cyclone, which is structured like a vertically distributed pair of vortices of opposite sign, would experience a mutual propagation if the vortex dipole is tilted. In particular, there are two ways to cause this kind of interaction.

1) The existence of ambient vertical shear: the background vertical wind shear acts to tilt the vortex pair by blowing the upper potential vorticity anomaly downshear. Evidence of this phenomenon has been found in Figs. 2c and (d) and also by Molinari (personal communication) in his IPV analyses of hurricanes. As the members of the vortex pair are displaced, they begin to interact with each other. Their mutual interaction will move the pair at right angles to the axis connecting them. On this basis, we infer that NH (SH) tropical cyclones should drift with respect to the mean winds in a direction to the left (right) of the background vertical shear vector.

2) The "β effect" on the upper anticyclone: the upper anticyclone drifts equatorward and westward due to the effect of the background potential vorticity gradient. Therefore, we suppose that the upper anticyclone, experiencing such a drift, would interact with the lower layer vortex and lead to an eastward and equatorward motion of the cyclone.

In this paper, we shall focus on the first effect.

3. Description of the model

a. *Background of the method of contour dynamics and contour surgery*

Contour dynamics is a Lagrangian computational method used to integrate flows associated with patches

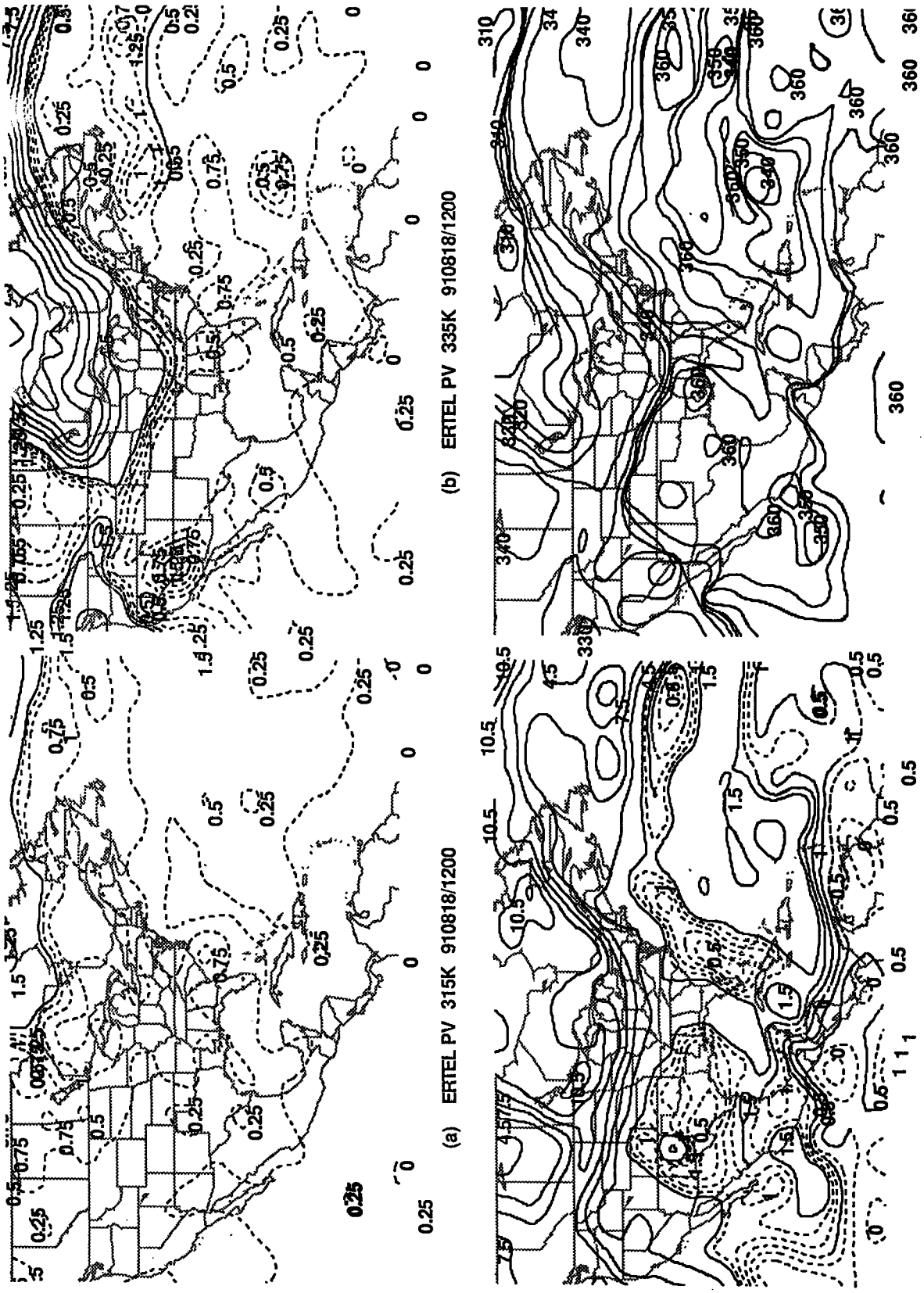

FIG. 2. Ertel potential vorticity and tropopause potential temperature fields at 1200 UTC 18 August 1991. Shown in (a) upper left, (b) upper right, and (c) lower left are the PV maps for the 315, 335, and 355 K isentropic surfaces, respectively. Potential vorticity values smaller than (larger than or equal to) 1.5 PVU are shown as dashed lines (solid lines) with contour intervals of 0.25 PVU (1.5 PVU). Shown in (d) lower right is the tropopause potential temperature (on the 1.5 PVU surface). The contour interval is 5 K.

of piecewise constant potential vorticity. This method leads to a closed dynamical system within which the evolution of the flow can be uniquely determined by the contours bounding the patches. (In practice, the contours are represented by a finite number of discrete nodes.) In other words, contour dynamics achieves its great numerical efficiency by integrating only on the contours instead of on the total potential vorticity field. To apply the contour-dynamics technique, the Green function associated with the differential operators of the fluid flow equations must be inverted. Because only certain fluid flows, such as barotropic, equivalent barotropic, or two-layer quasigeostrophic flows, have a simple enough mathematical form that their Green functions can be analytically found, the contour-dynamics technique is restricted mainly to applications on these flows. For example, using the method of contour dynamics, Polvani et al. (1989) performed an extensive study of geostrophic vortex dynamics in a two-layer quasigeostrophic model.

The method of contour surgery improves the resolution of the contour by adding nodes (called nodes adjustment) in regions of high curvature or smaller velocity. It is also more efficient and prevents unlimited enstrophy cascades to small scale by removing contour features (called contour adjustment) thinner than some prescribed tolerance. A detailed description of the methods of contour dynamics and contour surgery can be found in Dritschel (1989).

The primary disadvantage of contour dynamic is that it prohibits the existence of background potential vorticity gradients except on contours where finite potential vorticity jumps occur. Therefore, the contour dynamics approach inherently rules out the possibility of including a smooth planetary vorticity gradient. Although this makes the model somewhat unrealistic, it does allow us to isolate the effect of ambient vertical shear on tropical cyclone propagation. The other disadvantage of contour dynamics is that there is a time limit on the model integration, beyond which the number of nodes of the contour is too large to be integrated within a reasonable time.

b. *Background of the models*

A two-layer quasigeostrophic model is used to investigate the effect of background vertical shear. Since the two-layer model essentially assumes layers of constant density, diabatic effects cannot be explicitly included. For this reason, the forcing of potential vorticity from diabatic effects is specified. The approach we have taken is to simulate the interaction of a baroclinic vortex dipole with the background shear, using the methods of contour dynamics and contour surgery applied to a two-layer quasigeostrophic system.

We consider the simplest analog of a mature tropical cyclone to be a diabatically and frictionally maintained point vortex of constant strength in the lower layer and, in the upper layer, a patch of uniform, zero potential vorticity air surrounded by an infinite region of constant potential vorticity. The diabatic sink of potential vorticity in the upper layer is represented as the expansion of the area of the upper potential vorticity anomaly owing to a radial outward potential flow emanating from a point-mass source collocated with the lower vortex. According to the principle of mass continuity, the potential flow can be calculated from the lower boundary frictionally driven mass influx.

To isolate the effect of the ambient vertical shear, we explore the case of a vanishing ambient potential vorticity gradient. Therefore, the upper vortex patch is advected by the rotational flows (associated with both the upper-layer contour itself and the lower-layer vortex), the divergent flow (associated with the mass source), and the mean shear flow. The evolution of the upper vortex patch is integrated by the method of contour dynamics and contour surgery. This formulation is an ideally simple model for exploring the effects of vertical shear in isolation. The quasigeostrophic aspect of the model is a poor representation of the vertical penetration of the effect of potential vorticity anomalies near the storm center but should be adequate for describing the effect of the low-level cyclonic anomaly on the upper-level contour evolution at relatively large radius and for describing the downward penetration of the effect of the upper-level anomaly, whose associated rotational flow is probably weak enough to satisfy quasigeostrophy. We emphasize that the present work is meant to describe the first-order effects of vertical shear given the approximations inherent in the model.

c. *Formulation of the model equations*

In a continuous quasigeostrophic flow, the meridional gradient of zonal-mean pseudo–potential vorticity is

$$\frac{\partial \bar{q}}{\partial y} = \beta - \frac{\partial^2 \bar{U}}{\partial y^2} - \frac{f_0^2}{N^2}\left[\frac{\partial^2 \bar{U}}{\partial z^2} + \frac{1}{H}\frac{\partial \bar{U}}{\partial z}\right], \quad (3.1)$$

where $\bar{U}$ is the zonal mean wind, f_0 is the Coriolis parameter evaluated in the middle of the domain, N is the Brunt–Väisälä frequency, and H is a scale height defined as

$$H = \left[-\frac{\rho}{N^2}\frac{\partial (N^2/\rho)}{\partial z}\right]^{-1},$$

where ρ is the mean density; N^2 and ρ may vary only with altitude.

The aforementioned observations suggest that, at least in the subtropics, the meridional gradient of mean pseudo–potential vorticity is much smaller than β. For this reason and in order to isolate the direct effect of vertical wind shear on storm propagation, we take

$$\frac{\partial \bar{q}}{\partial y} = 0,$$

and

$$\frac{\partial \bar{U}}{\partial y} = 0.$$

By Eq. (3.1), then, we are constrained to use a vertical profile of $\bar{U}$ that satisfies

$$\frac{d^2\bar{U}}{dz^2} + \frac{1}{H}\frac{d\bar{U}}{dz} - \frac{N^2\beta}{f_0^2} = 0. \tag{3.2}$$

Taking N^2 to be approximately constant, the zonal wind profile that satisfies this is

$$\bar{U} = U_0 + \left(U_T - U_0 - \frac{N^2H^2}{f_0^2}\beta\right)\left(\frac{e^{-z/H} - 1}{e^{-1} - 1}\right) + \left(\frac{N^2H^2}{f_0^2}\right)\beta\left(\frac{z}{H}\right),$$

where $U_T = \bar{U}$ (at $z = H$) and $U_0 = \bar{U}$ (at $z = 0$). If it is further required that the surface meridional temperature vanishes [i.e., $d\bar{U}/dz$ (at $z = 0$) $= 0$], as is approximately true in the tropics, then

$$\bar{U} = U_0 + \frac{N^2H^2}{f_0^2}\beta\left(e^{-z/H} - 1 + \frac{z}{H}\right).$$

This profile has very little shear through most of the troposphere, with an increasing shear near the tropopause. For typical values of the parameters, this would give an increase of about 10 m s^{-1} between the mean surface zonal wind and the wind at the tropopause. (This mean shear could be reduced to zero if a weak easterly shear near the surface is assumed.)

In a two-layer representation, it is not possible to represent in a direct way the curvature of the mean wind profile, but the mean meridional gradient of potential vorticity can be canceled out by introducing upper and lower boundaries with gentle meridional slopes. When this is done, the conservation equations for pseudo-potential vorticity in each layer become

$$\frac{dq_1}{dt} = \left[\frac{\partial}{\partial t} + J(\Psi_1, *)\right]q_1 = H_1, \tag{3.3}$$

$$\frac{dq_2}{dt} = \left[\frac{\partial}{\partial t} + J(\Psi_2, *)\right]q_2 = H_2 + F_2, \tag{3.4}$$

where subscripts 1 and 2 denote the upper and lower layer, respectively, and

$$q_1 = \nabla^2\Psi_1 + \frac{\Psi_2 - \Psi_1}{L_R^2} + f_0 + \beta_1 y,$$

$$q_2 = \nabla^2\Psi_2 + \epsilon\frac{\Psi_1 - \Psi_2}{L_R^2} + f_0 + \beta_2 y,$$

where Ψ_1 and Ψ_2 are the streamfunctions in the upper and lower layers, respectively; H_1 is the diabatic source of potential vorticity in the upper layer; H_2 is the diabatic source in the lower layer; F_2 is the frictional dissipation of potential vorticity at the lower boundary; L_R is the radius of deformation ($L_R = (gD_1\Delta\rho/\rho)^{1/2}/f_0$); D_1 is the depth of the upper layer; $\Delta\rho$ is the density difference between the two layers; f_0 is the local Coriolis parameter; and β_1 and β_2 are the mean potential vorticity gradients in the upper and lower layers, respectively. These are given by

$$\beta_1 \equiv \beta - \frac{f_0\alpha_1}{D_1}, \tag{3.5}$$

$$\beta_2 \equiv \beta + \frac{f_0\alpha_2}{D_2}, \tag{3.6}$$

where α_1 and α_2 are the slopes of the upper and lower boundaries, respectively.

The Jacobian and Laplacian operators are given by

$$J(A, B) \equiv \frac{\partial A}{\partial x}\frac{\partial B}{\partial y} - \frac{\partial A}{\partial y}\frac{\partial B}{\partial x},$$

$$\nabla^2 = \frac{\partial^2}{\partial x^2} + \frac{\partial^2}{\partial y^2},$$

and $\epsilon = D_1/D_2$ is the ratio of the upper to lower layer thickness (when the fluid is at rest).

The flow is divided into two parts:

1) a mean zonal flow (denoted by overbars), which is taken here to be independent of y, and

2) vortical disturbances associated with the potential vorticity anomalies (denoted by primes), that is,

$$\Psi_1 = \bar{\Psi}_1 + \Psi_1' = -\int \bar{U}_1 dy + \Psi_1',$$

$$\Psi_2 = \bar{\Psi}_2 + \Psi_2' = -\int \bar{U}_2 dy + \Psi_2'.$$

Then (3.3) and (3.4) become

$$\left(\frac{\partial}{\partial t} + \bar{U}_1\frac{\partial}{\partial x}\right)q_1' + J(\Psi_1', \bar{q}_1 + q_1') = H_1, \tag{3.7}$$

$$\left(\frac{\partial}{\partial t} + \bar{U}_2\frac{\partial}{\partial x}\right)q_2' + J(\Psi_2', \bar{q}_2 + q_2') = H_2 + F_2, \tag{3.8}$$

where

$$\bar{q}_1 = f_0 + \left(\beta_1 + \frac{\bar{U}_1 - \bar{U}_2}{L_R^2}\right)y,$$

$$\bar{q}_2 = f_0 + \left(\beta_2 - \epsilon\frac{\bar{U}_1 - \bar{U}_2}{L_R^2}\right)y,$$

and

$$q_1' = \nabla^2\Psi_1' + \frac{\Psi_2' - \Psi_1'}{L_R^2},$$

$$q_2' = \nabla^2\Psi_2' + \epsilon\frac{\Psi_1' - \Psi_2'}{L_R^2}.$$

To be able to apply contour dynamics, we require that the mean potential vorticity gradient vanishes, that is,

$$\frac{d\bar{q}_1}{dy} = \frac{\bar{U}_1 - \bar{U}_2}{L_R^2} + \beta_1 = 0,$$

$$\frac{d\bar{q}_2}{dy} = \epsilon \frac{\bar{U}_2 - \bar{U}_1}{L_R^2} + \beta_2 = 0.$$

Using (3.5) and (3.6), this determines the slopes of the two boundaries:

$$\alpha_1 = \frac{D_1}{f_0}\left(\beta + \frac{\bar{U}_1 - \bar{U}_2}{L_R^2}\right),$$

$$\alpha_2 = \frac{D_2}{f_0}\left(-\beta + \epsilon \frac{\bar{U}_1 - \bar{U}_2}{L_R^2}\right).$$

Typical values of α_1 and α_2 are 1×10^{-3} and -1×10^{-3}, respectively. Thus, we are free to choose $\bar{U}_1$ and $\bar{U}_2$, the mean flow velocities in the upper and lower layers. This does not violate the spirit of our analysis, which constrains the flow to have no mean gradient of pseudo-potential vorticity. As seen earlier, this requirement determines the curvature of the flow profile and not its mean shear.

d. Model simplifications

1) As there is no mean gradient of potential vorticity, the system becomes Galilean-invariant, and we can further assume no mean wind in the lower layer, that is, $\bar{U}_2 = 0$.

2) Real hurricanes contain highly concentrated potential vorticity anomalies at the center. This is idealized as a point potential vortex in the lower layer. Therefore, in the lower layer, we assume that a mature tropical cyclone is diabatically and frictionally maintained and represent it there as a point vortex of constant strength S_2, that is,

$$q_2' = S_2\delta(\mathbf{x} - \mathbf{x}_p(t)),$$

where $\mathbf{x}_p$ is the position of the point vortex, and

$$H_2 + F_2 = 0.$$

The last relation is based on the assumption that the destruction of potential vorticity by friction is balanced by its creation by diabatic heating. This representation makes the cyclone drift quite visible (i.e., the cyclone drift is simply the movement of the point vortex).

3) In the upper layer, the upward decrease of diabatic heating causes the potential vorticity associated with the anticyclone to decrease with time. We represent this by a patch of constant, negative potential vorticity anomaly, whose area expands owing to a radial outward potential flow, emanating from a point mass source collocated with the lower vortex. In other words, the forcing is represented as an advection of the potential vorticity by a potential flow $\mathbf{u}_p$. Therefore,

$$H_1 = -\mathbf{u}_p \cdot \nabla q_1',$$

$$q_1' = Q_1 X_D(\mathbf{x}),$$

where Q_1 is the potential vorticity jump across the contour associated with a patch domain D, and X is a symbol for the generalized step function, that is,

$$X_D(\mathbf{x}) = 1, \quad \text{when} \quad \mathbf{x} \in D,$$

$$X_D(\mathbf{x}) = 0, \quad \text{when} \quad \mathbf{x} \notin D.$$

Then (3.7) and (3.8) can be rewritten (neglecting the prime symbol) as

$$\left(\frac{\partial}{\partial t} + \bar{U}_1 \frac{\partial}{\partial x} + \mathbf{u}_p \cdot \nabla\right) q_1 + J(\Psi_1, q_1) = 0, \quad (3.9)$$

$$\frac{\partial}{\partial t} q_2 + J(\Psi_2, q_2) = 0, \quad (3.10)$$

where

$$q_1 = \nabla^2\Psi_1 + \frac{\Psi_2 - \Psi_1}{L_R^2} = Q_1 X_D(\mathbf{x}),$$

$$q_2 = \nabla^2\Psi_2 + \epsilon \frac{\Psi_1 - \Psi_2}{L_R^2} = S_2\delta(\mathbf{x} - \mathbf{x}_p(t)).$$

e. Estimation of the potential flow

In general, the transverse circulation of a mature hurricane consists of radial inflow within the frictional boundary layer, ascent within a narrow outward sloping eyewall, and radial outward flow in a thin layer at the top of the storm. From this point of view, the potential radial outward flow in our model can be approximated as a flow emanating from a mass source in the upper layer, whose mass flux is determined by the surface frictionally induced inflow. Considering an axisymmetric hurricane, the angular momentum M is defined as

$$M = rv + \frac{fr^2}{2},$$

where r is the distance from the storm center. The azimuthal component of the momentum equation in the surface inflow layer in cylindrical coordinates is

$$u \frac{\partial M}{\partial r} = -rg \frac{\partial \tau}{\partial p},$$

or

$$u\left[f_0 + \frac{1}{r}\frac{\partial (rv)}{\partial r}\right]r = -rg \frac{\partial \tau}{\partial p}, \quad (3.11)$$

where u and v are the radial and azimuthal components of the wind, respectively, f is approximated by the local

Coriolis parameter f_0, and τ is the azimuthal component of frictional stress. We examine (3.11) at a particular radius r_c, where the relative vorticity ζ changes sign, that is,

$$\zeta = \left[\frac{1}{r}\frac{\partial(rv)}{\partial r}\right]_{r=r_c} = 0.$$

At this radius (3.11) becomes

$$uf_0 r_c = -r_c g \frac{\partial \tau}{\partial p}.$$

Integrating vertically over the surface boundary layer, we get

$$\int uf_0 r_c \frac{dp}{g} = -r_c \tau_s,$$

where τ_s is the azimuthal component of surface frictional stress at radius r_c. By applying the bulk aerodynamic formula,

$$\tau_s = \rho_s c_D v_c |v_c|,$$

where c_D is the drag coefficient and v_c is the azimuthal surface wind at radius r_c, the total mass influx is

$$F_{\text{in}} = \left|2\pi r_c \int \rho u dz\right| = \left|2\pi r_c \int u \frac{dp}{g}\right| = \frac{2\pi\rho_s r_c c_D v_c^2}{f_0}, \tag{3.12}$$

where the hydrostatic equation is used. Also, the outward mass flux in the upper layer can be represented as

$$F_{\text{out}} = 2\pi\rho_1 u_p r_1 D_1, \tag{3.13}$$

where u_p is the outward radial wind at radius r_1 in the upper layer and ρ_1 is a mean density in the upper layer. By equating F_{in} and F_{out}, the potential flow

$$u_p = \frac{\rho_s r_c c_D v_c^2}{f_0 \rho_1 r_1 D_1}$$

is obtained.

f. Scaling of the model

We choose physical scaling parameters such that the normalized governing equations can be described by only a few nondimensional parameters. To do this, the following scales are chosen:

- horizontal length scale $L = r_c$, which is the radius where the surface relative vorticity of the storm changes sign (a typical value is 500 km);
- horizontal velocity scale $U = \rho_s c_D v_c^2/(\rho_1 f_0 D_1)$, which is the frictionally induced potential flow speed in the upper layer at $r_1 = r_c$ (a typical value is 1 m s^{-1}).

Then, by using the advective time scale (a typical value of 5 days), (3.9) and (3.10) can be expressed in nondimensional form as

$$\left[\frac{\partial}{\partial t} + (\chi + \mu)\frac{\partial}{\partial x} + v\frac{\partial}{\partial y}\right] q_1 + J(\Psi_1, q_1) = 0, \tag{3.17}$$

$$\frac{\partial}{\partial t} q_2 + J(\Psi_2, q_2) = 0, \tag{3.18}$$

where

$$q_1 = \nabla^2\Psi_1 + \gamma^2(\Psi_2 - \Psi_1) = \prod_1 X_D(\mathbf{x}),$$

$$q_2 = \nabla^2\Psi_2 + \epsilon\gamma^2(\Psi_1 - \Psi_2) = \prod_2 \delta(\mathbf{x} - \mathbf{x}_p(t)),$$

and

$\prod_1 = Q_1 r_c \rho_1 f_0 D_1/(\rho_s c_D v_c^2)$: the nondimensional upper-layer potential vorticity jump,

$\prod_2 = S_2\rho_1 f_0 D_1/(\rho_s c_D v_c^2 r_c) = 2\pi\rho_1 f_0 D_1/(\rho_s c_D v_c)$: the nondimensional lower-layer vortex strength,

where we have approximated the strength of the lower-layer hurricane vortex as $S_2 = 2\pi v_c r_c$,

$\gamma = r_0/L_R$: the ratio of the horizontal length scale to the radius of deformation,

$\chi = \bar{U}_1\rho_1 f_0 D_1/(\rho_s c_D v_c^2)$: the nondimensional upper-layer mean wind,

$\mu = (x - x_p)/r_1(\mathbf{x})$: the nondimensional zonal component of the potential flow,

$\nu = (y - y_p)/r_1(\mathbf{x})$: the nondimensional meridional component of the potential flow, where

$\mathbf{x} = (x, y)$, $\mathbf{x}_p = (x_p, y_p)$ and $r_1(\mathbf{x}) = [(x - x_p)^2 + (y - y_p)^2]^{1/2}$.

Equations (3.17) and (3.18) are the final forms of the governing equations. The behavior of the model is governed by the following five dimensionless parameters:

$$\epsilon = \frac{D_1}{D_2},$$

$$\gamma = \frac{r_c f_0}{(gD_1\Delta\rho/\rho)^{1/2}},$$

$$\chi = \frac{\bar{U}_1\rho_1 f_0 D_1}{\rho_s c_D v_c^2},$$

$$\prod_1 = \frac{Q_1 r_c \rho_1 f_0 D_1}{\rho_s c_D v_c^2},$$

$$\prod_2 = \frac{2\pi\rho_1 f_0 D_1}{\rho_s c_D v_c}.$$

4. Results

a. Control experiments

We start our model integration by specifying the position of a point vortex in the lower layer, with a circular

patch of zero potential vorticity in the upper layer, whose center is collocated with the surface vortex. The dimensionless radius of the initially circular contour of upper-level potential vorticity patch is $r_n = r_i/r_c$. For convenience, only the NH case is studied.

The model is begun by specifying a lower point vortex whose strength Π_2 is consistent with a vortex characterized by $r_c = 500$ km, $v_c = 10$ m s^{-1}, $D_1 = 2$ km, and an upper-layer vortex patch of radius $r_n = 0.3$, with a strength Π_1 given by taking $Q_1 = -f_0$ (i.e., the anomaly has zero potential vorticity and the environment has potential vorticity f_0). We take the value of f_0 at 20° latitude, $c_D = 1 \times 10^{-3}$, and $\epsilon = 0.25$. By choosing $\Delta\rho/\rho$ to be 0.05, which is equivalent to an atmosphere of the same vertical depth with uniform static stability $N^2 = 1 \times 10^{-4}$ s^{-2}, the value of γ is 0.79, and the corresponding values of Π_1 and Π_2 are 25 and 62.83. Control experiments were performed by integrating the model to nondimensional time $t = 4$, with westerly vertical shear (χ) varying from 0 to 10.

For the case with no vertical shear ($\chi = 0$), it is found, as expected, that the upper patch expands with time and remains circularly symmetric and that there is no lower vortex movement. The wind distributions at time $t = 4$ in each layer (Figs. 3 and 4) show that the upper flow is anticyclonic and outward, similar to a real hurricane outflow, and the lower-layer flow is symmetric around the vortex center, so that no vortex drift is induced.

Next the case with weak shear is investigated, that is, $\chi = 1.25$ (this corresponds to an upper-layer mean wind of approximately 1.25 m s^{-1}). The evolution of the upper-level contour for this case is shown in Fig. 5. It is found that the vortex patch expands and is advected downshear. Also, roll-up of the vortex patch occurs on the downshear side, essentially due to barotropic instability. The evolution of the vortex zonal and meridional drift velocity and total drift speed with time (Figs. 6, 7 and 8) shows that the vortex drift is mainly meridional and increases with time. The induced zonal drift, though smaller in magnitude, is mainly associated with the roll-up of the vortex patch, which, after a certain integration time, is located eastward and southward of the lower vortex.

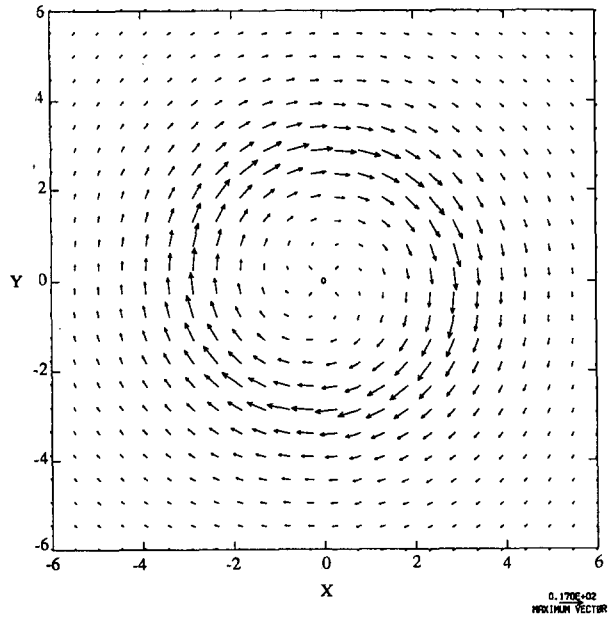

FIG. 3. The upper-layer wind distribution at time $t = 4$ for $\epsilon = 0.25$, $\gamma = 0.79$, and $\chi = 0$. The lower vortex is located in the center and is shown as "O." One unit length in the domain corresponds to 500 km.

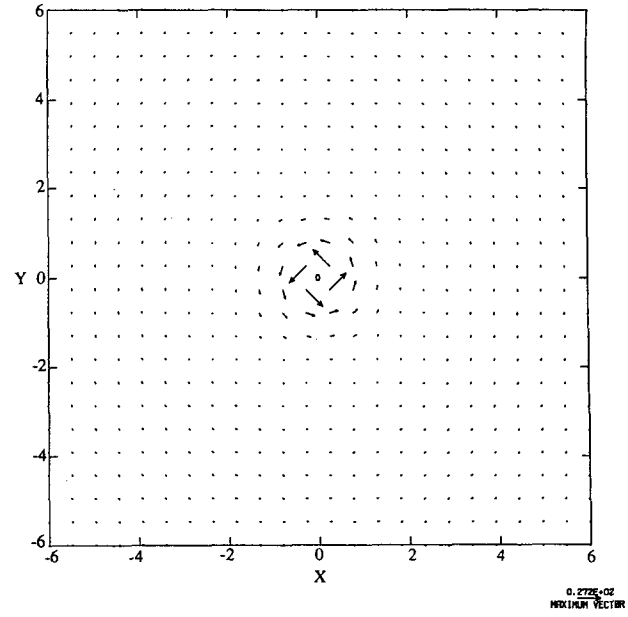

FIG. 4. The lower-layer wind distribution at time $t = 4$ for $\epsilon = 0.25$, $\gamma = 0.79$, and $\chi = 0$. The lower vortex is located in the center and is shown as "O." One unit length in the domain corresponds to 500 km.

The maximum dimensional drift speed (approximately 3 m s^{-1}) in this case is comparable in magnitude with that associated with β drift (cf. Chan and Williams 1987). A recent study of hurricane motion in a three-layer model by Shapiro (1992) indicated that the existence of ambient westerly shear advects the upper-layer negative potential vorticity anomaly downshear and thus induces an anticyclonic anomaly that advects the middle-layer vortex. Shapiro concluded that this effect is secondary to the β effect. Our results, however, suggest that the background shear can be important in causing the hurricane movement, though we have excluded the influence of any background potential vorticity gradient.

For cases with very little shear, for example, $\chi = 0.25$, the vortex patch simply rotates around the lower point vortex (Fig. 9), and the drift velocity wavers with time with an upper bound (Figs. 6, 7, and 8). In these cases, more eastward vortex drift is found.

For cases with larger shear, for example, $\chi = 5$, the

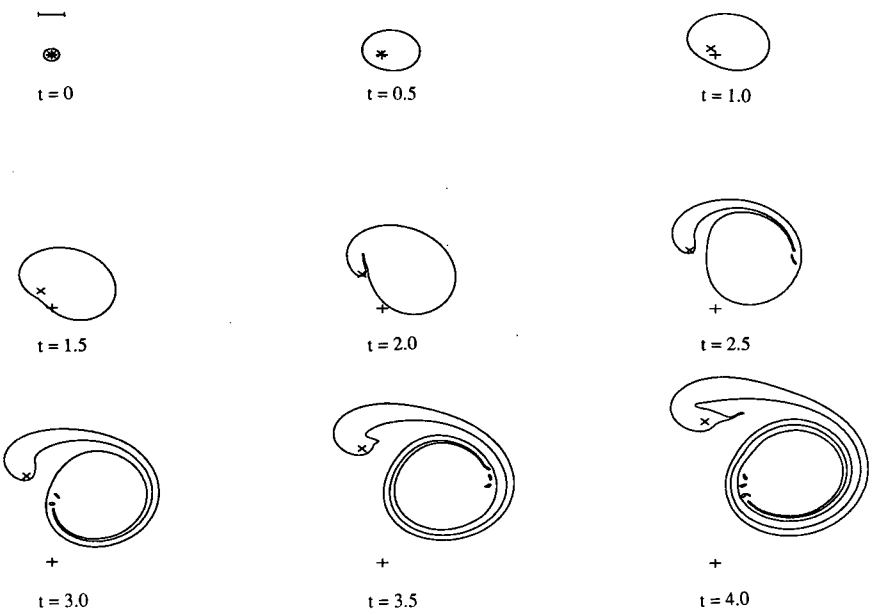

FIG. 5. The evolution of the upper-layer vortex patch for $\epsilon = 0.25$, $\gamma = 0.79$, and $\chi = 1.25$. The lower-layer point vortex is shown as "×." The initial position of the point vortex is indicated as "+." The time interval between each plot is 0.5. The unit length scale (500 km) is shown in the upper left corner.

patch is rapidly advected downshear and becomes zonally elongated (Fig. 10). The low potential vorticity anomaly behaves more like a passive plume. Since the bulk of the upper vortex patch is far from the lower vortex, its influence on the lower vortex is limited, so that the induced vortex drift speed reaches a nearly quasi-steady state (Figs. 6, 7, and 8). In these cases, the elongation of the potential vorticity anomaly leads to barotropic instability and the filamentation in the middle of the contour strip. However, strong roll-up of the contour occurs at the downshear end of the anomaly.

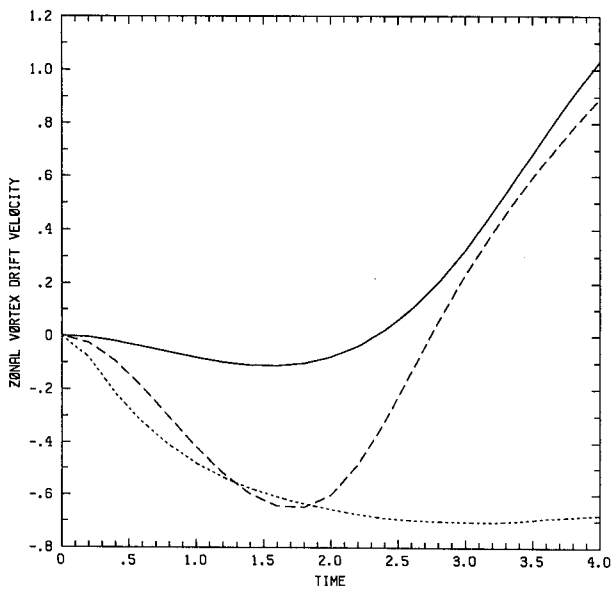

FIG. 6. The evolution of induced lower-layer vortex zonal velocity with time for $\epsilon = 0.25$, $\gamma = 0.79$, and $\chi = 0.25$ (solid line); for $\chi = 1.25$ (long-dashed line); and for $\chi = 5$ (short-dashed line).

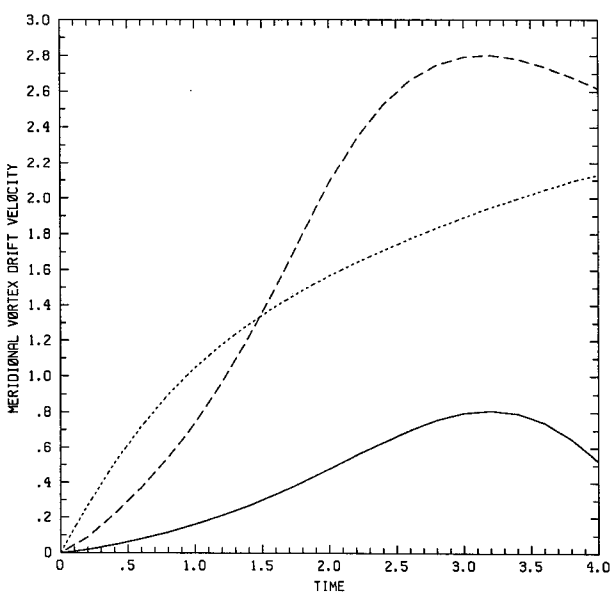

FIG. 7. The evolution of induced lower-layer vortex meridional velocity with time for $\epsilon = 0.25$, $\gamma = 0.79$, and $\chi = 0.25$ (solid line); for $\chi = 1.25$ (long-dashed line); and for $\chi = 5$ (short-dashed line).

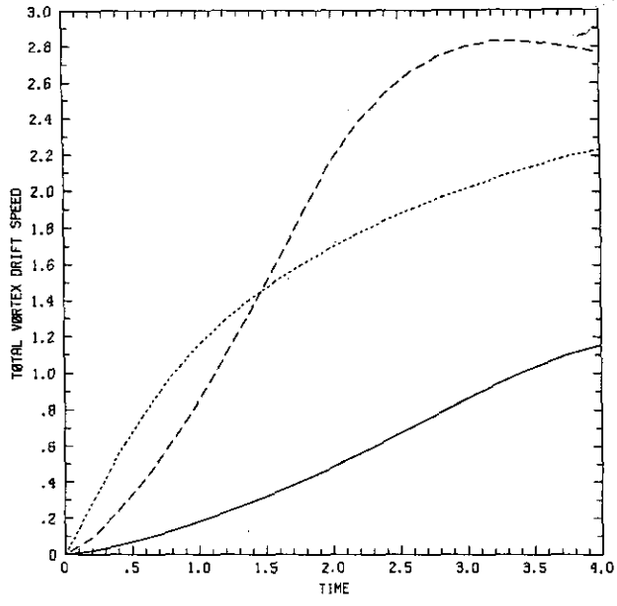

FIG. 8. The evolution of induced lower-layer vortex total speed with time for $\epsilon = 0.25$, $\gamma = 0.79$, and $\chi = 0.25$ (solid line); for $\chi = 1.25$ (long-dashed line); for $\chi = 5$ (short-dashed line).

The trajectories of the lower vortex in the aforementioned three experiments are shown in Fig. 11. In all cases, distinct northward vortex drifts associated with different magnitudes of the mean westerly shears are found, as expected. Also, the drift in the zonal direction is a function of the background shear, that is, more eastward drift is associated with weaker shear. Figure 12 shows the maximum total drift speed as a function of the ambient shear. The vortex drift initially increases as the shear increases, and there exists an optimal shear (about $\chi = 1.25$ for these parameter values) that maximizes the vortex drift. Above that optimal shear, the drift speed decreases with increasing shear and approaches a constant.

b. Other sensitivity experiments

We have performed two sets of experiments to determine the sensitivity of the vortex motion to the thickness ratio of the two layers (ϵ). The first set of experiments were conducted by choosing ϵ to be 1, with χ varying from 0 to 10. Figures 13, 14, 15, and 16 show the evolution with time of the zonal vortex drift velocity, the meridional vortex drift velocity, the total vortex drift speed, and the trajectories of the lower vortex for cases with $\chi = 1$, 3, and 5. For relatively weak shear ($\chi = 1$), the induced drift speed wavers with time. The vortex moves northeastward initially, then moves southeastward with a cycloid-like trajectory. For other cases, the result behaves like the control experiments, except that more drift is induced, the "optimal shear" (see Fig. 17) is shifted to higher value, and the induced drift does not drop much when the ambient shear increases above the "optimal shear."

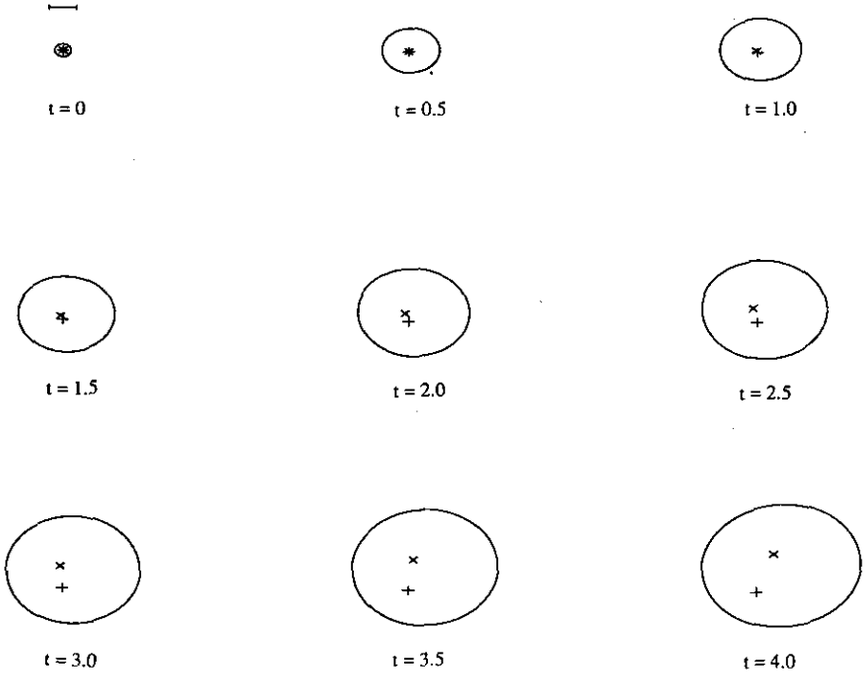

FIG. 9. The evolution of the upper-layer vortex patch for $\epsilon = 0.25$, $\gamma = 0.79$, and $\chi = 0.25$. The lower-layer point vortex is shown as "×." The initial position of the point vortex is indicated as "+." The time interval between each plot is 0.5. The unit length scale (500 km) is shown in the upper left corner.

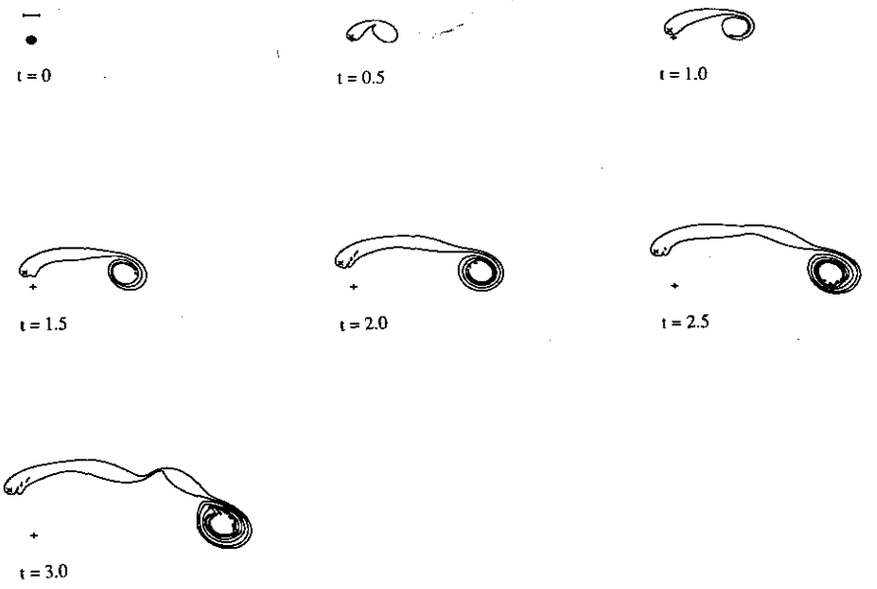

FIG. 10. The evolution of the upper-layer vortex patch for $\epsilon = 0.25$, $\gamma = 0.79$, and $\chi = 5$. The lower-layer point vortex is shown as "×." The initial position of the point vortex is indicated as "+." The time interval between each plot is 0.5. The unit length scale (500 km) is shown in the upper left corner.

The second set of experiments was performed by choosing ϵ to be 0.5. The results (not shown) are consistent with the control experiments, with a moderate increase in vortex drift.

The variation of the maximum induced drift speed and its velocity vector with parameters χ and ϵ (Figs. 17a and b) shows that both the maximum induced vortex speed and "optimal shear" increase with the value of ϵ. These results suggest that the drift induced by the interaction effect is quite sensitive to the thickness ratio of the two layers. What happens physically is that increases of ϵ strengthen the influence of the upper-layer potential vorticity anomaly on the lower-layer vortex and thus induce more vortex movement.

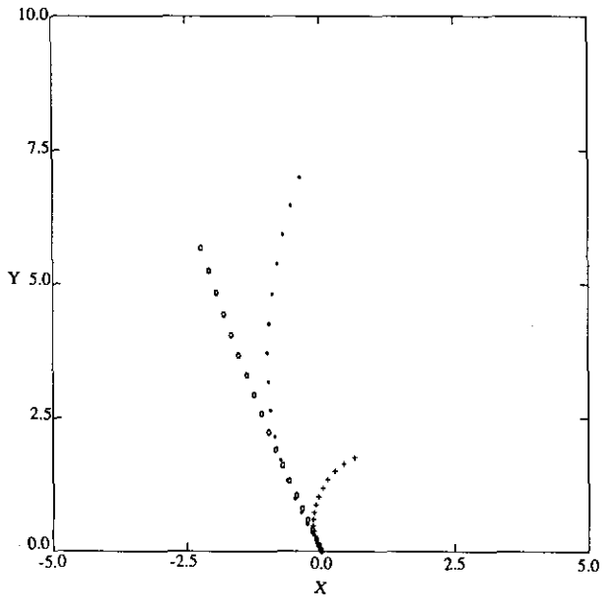

FIG. 11. Trajectories (units of 500 km) of the lower-layer vortex for $\epsilon = 0.25$, $\gamma = 0.79$, and $\chi = 0.25$ (shown as "+"); $\chi = 1.25$ (shown as "*"); and $\chi = 5$ (shown as "O").

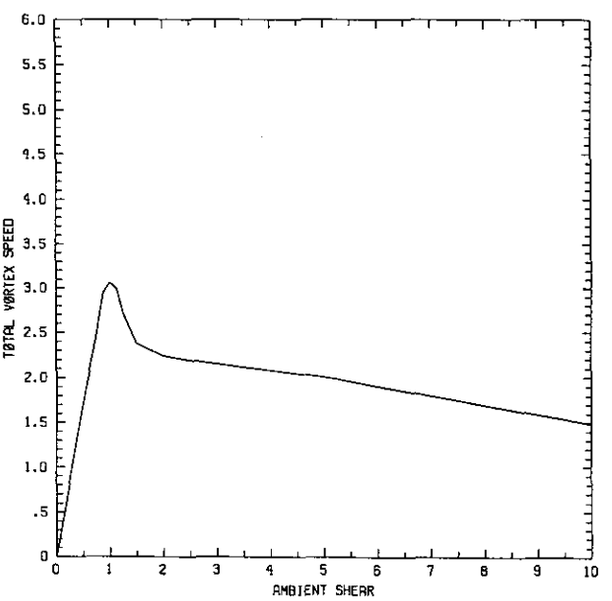

FIG. 12. The relation between the maximum induced vortex speed and the magnitude of the vertical shears (χ) for $\epsilon = 0.25$ and $\gamma = 0.79$.

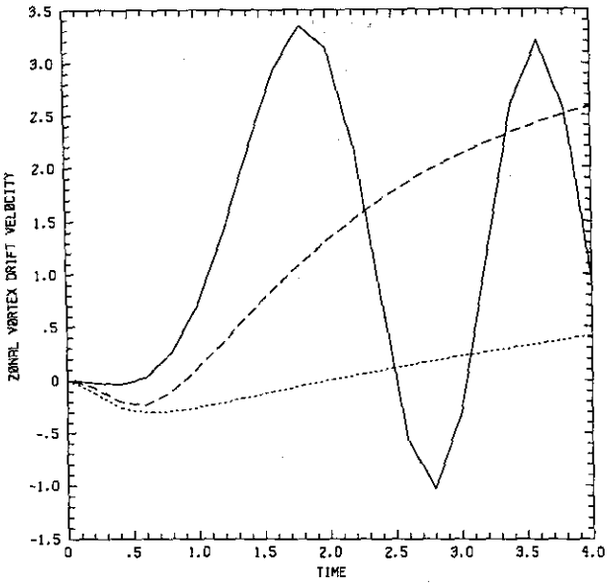

FIG. 13. The evolution of induced lower-layer vortex zonal velocity with time for $\epsilon = 1$, $\gamma = 0.79$, and $\chi = 1$ (solid line); for $\chi = 3$ (long-dashed line); and for $\chi = 5$ (short-dashed line).

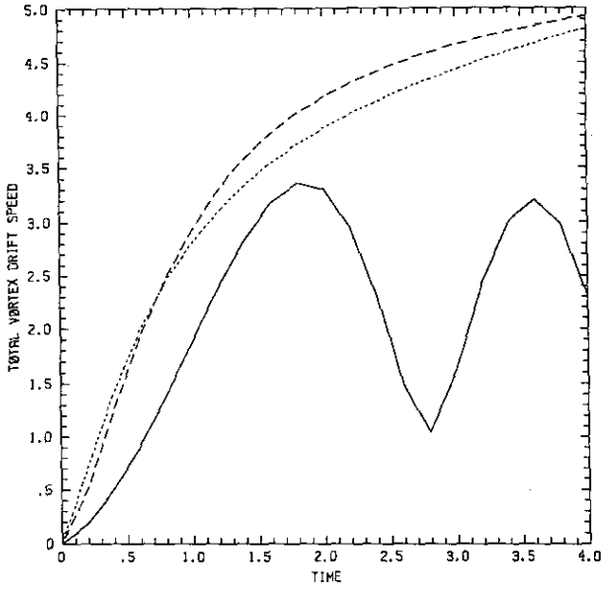

FIG. 15. The evolution of induced lower-layer vortex total speed with time for $\epsilon = 1$, $\gamma = 0.79$, and $\chi = 1$ (solid line); for $\chi = 3$ (long-dashed line); and for $\chi = 5$ (short-dashed line).

Two other experiments are performed to test the model sensitivity to the ratio of the horizontal length scale to the radius of deformation (γ). We run the model with γ equal to 1 and 0.5, respectively, with varying values of χ. The variations of the maximum induced drift speed and its velocity vector with the parameters χ and γ are shown in Figs. 18a and 18b. The result suggests that the maximum vortex drift is relatively insensitive to the parameter γ. Though the parameter γ reflects the degrees to which the upper and lower layers are coupled, its quantitative influence on vortex motion appears as a coefficient in the modified Bessel function of the second kind, of order one (K_1), whose value is quite insensitive to the choice of γ.

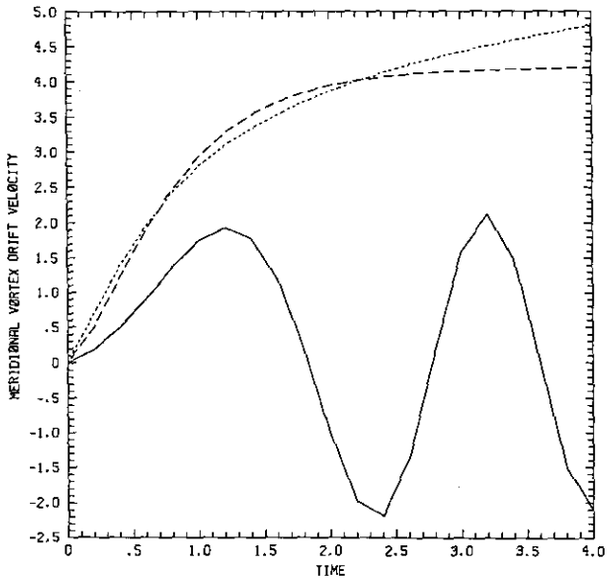

FIG. 14. The evolution of induced lower-layer vortex meridional velocity with time for $\epsilon = 1$, $\gamma = 0.79$, and $\chi = 1$ (solid line); for $\chi = 3$ (long-dashed line); and for $\chi = 5$ (short-dashed line).

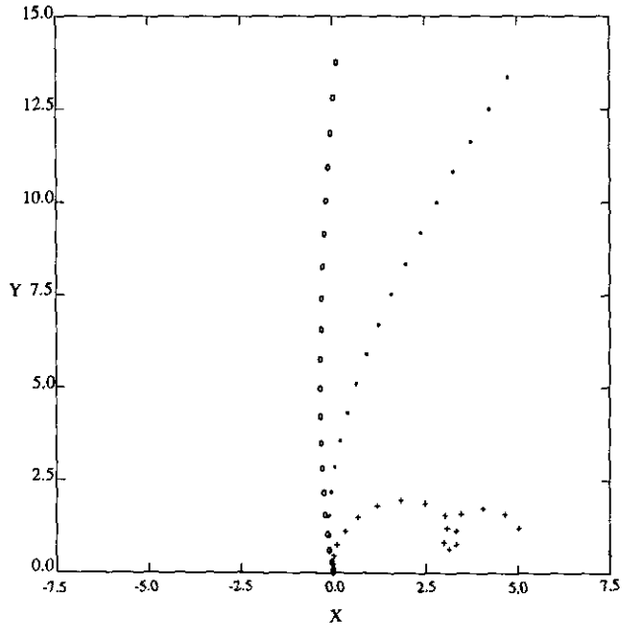

FIG. 16. Trajectories (units of 500 km) of the lower-layer vortex for $\epsilon = 1$, $\gamma = 0.79$, and $\chi = 1$ (shown as "+"); $\chi = 3$ (shown as "*"); and $\chi = 5$ (shown as "O").

Final experiments were performed to test the sensitivity to the parameters Π_1 and Π_2, and the initial radius of the upper patch, r_n. We find that an initial lower vortex of different strength or a upper vortex patch with different initial area has little influence on the eventual movement of the vortex. An initial upper vortex patch with higher potential vorticity jump tends to have more vortex drift. This relation is nearly linear. This result indicates, as one would expect, that a hurricane surmounted by a stronger negative potential vorticity anomaly would experience more interaction between the upper and lower vortices.

5. Summary

Observations show that tropical cyclones have broad anticyclones aloft and that the distribution of potential vorticity gradient in the tropical atmosphere is highly inhomogeneous. There is some indication that the potential vorticity gradients in the subtropical troposphere are very weak, perhaps having been rendered so by the action of synoptic-scale disturbances. To account for this and to isolate the direct effect of vertical wind shear on the motion of a baroclinic vortex, we have performed experiments with an idealized two-layer quasi-geostrophic model in which there is no background potential vorticity gradient. The lower-layer potential vorticity anomaly is represented by a point vortex, while the upper-layer anomaly is represented by a patch of zero potential vorticity air, which is expanding in time owing to a point source of mass collocated with the lower-layer point potential vortex. The method of contour dynamics and contour surgery is used to integrate the upper-level pseudo-potential vorticity equation.

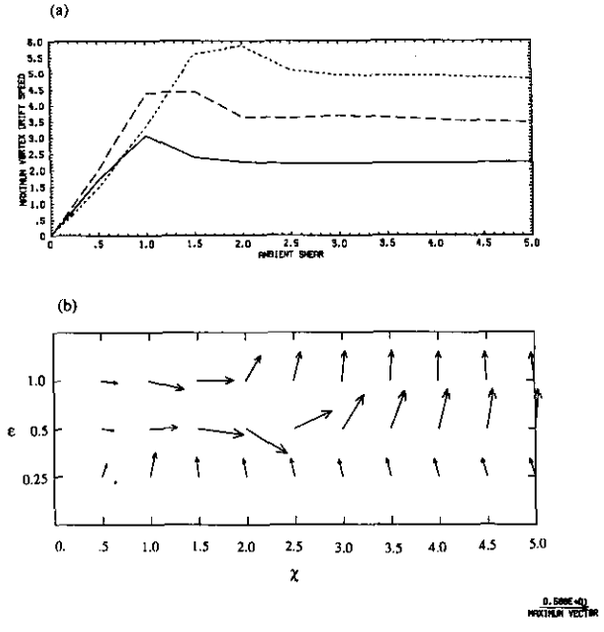

FIG. 17. (a) The relation between the maximum induced vortex speed and the magnitude of the vertical shears (χ) for $\gamma = 0.79$ and $\epsilon = 0.25$ (solid line); $\epsilon = 0.5$ (long-dashed); $\epsilon = 1$ (short-dashed). (b) The maximum induced vortex velocity vector as a function of the magnitude of χ and ϵ for $\gamma = 0.79$.

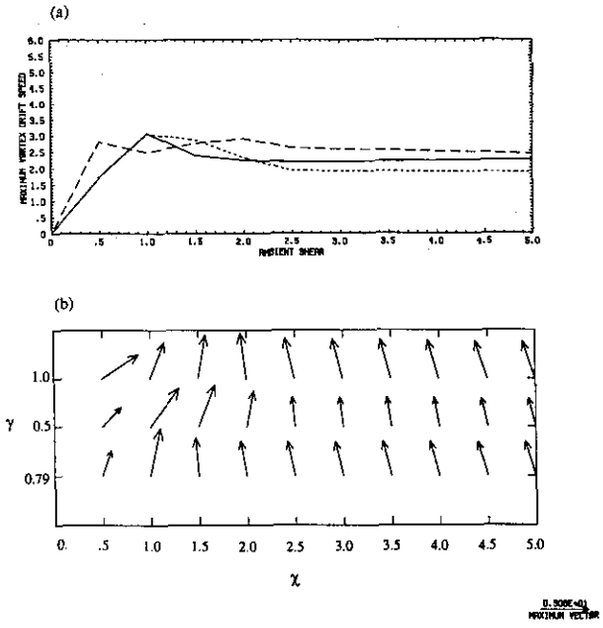

FIG. 18. (a) The relation between the maximum induced vortex speed and the magnitude of the vertical shears (χ) for $\epsilon = 0.25$ and $\gamma = 0.79$ (solid-line); $\gamma = 0.5$ (long-dashed line); and $\gamma = 1$ (short-dashed). (b) The maximum induced vortex velocity vector as a function of the magnitude of χ and γ for $\epsilon = 0.25$.

We find that the direct effect of ambient vertical shear is to displace the upper-level plume of anticyclonic relative potential vorticity downshear from the lower-layer cyclonic point potential vortex, thus inducing a mutual interaction between the circulations associated with each other. This results in a drift of the point vortex broadly to the left of the vertical shear vector (in the Northern Hemisphere). This drift is sensitive to the assumed relative thicknesses of the two layers, but its magnitude is generally comparable to that found in simulations of barotropic vortices on the β plane.

We feel that it is necessary to examine these effects using more comprehensive modeling and observational studies, with a view toward establishing the actual background potential vorticity gradients in the atmosphere. We are in the process of developing more complete models that also incorporate variable background potential vorticity gradients. We believe that this work will aid in improving our basic understanding of the factors influencing tropical cyclone motion and perhaps lead to better observational strategies for future forecasts of tropical cyclone motion.

Acknowledgments. The authors would like to thank Dr. Steve Meacham for providing the original two-layer contour dynamics code. We thank Dr. Glenn Flierl for

providing the computer facility. We also thank Drs. William Gray and Lloyd Shapiro for helpful comments on this paper. This research is supported through the National Science Foundation by Grant ATM-8815008.

REFERENCES

Anthes, R. A., and J. E. Hoke, 1975: The effect of horizontal divergence and latitudinal variation of the Coriolis parameter on the drift of a model hurricane. *Mon. Wea. Rev.*, **103,** 757–763.

Bretherton, F. P., 1966: Critical layer instability in baroclinic flows. *Quart. J. Roy. Meteor. Soc.*, **92,** 325–334.

Carr, L. E., and R. L. Elsberry, 1990: Observational evidence for tropical cyclone propagation relative to environmental steering. *J. Atmos. Sci.*, **47,** 542–546.

Chan, J. C.-L., and W. M. Gray, 1982: Tropical cyclone movement and surrounding flow relationship. *Mon. Wea. Rev.*, **110,** 1354–1376.

——, and R. T. Williams, 1987: Analytic and numerical studies of the beta-effect in tropical cyclone motion. Part 1. Zero mean flow. *J. Atmos. Sci.*, **44,** 1257–1264.

Davis, C. A., and K. A. Emanuel, 1991: Potential vorticity diagnostics of cyclogenesis. *Mon. Wea. Rev.*, **119,** 1929–1953.

DeMaria, M., 1985: Tropical cyclone motion in a nondivergent barotropic model. *Mon. Wea. Rev.*, **113,** 1199–1210.

Dong, K., and C. J. Neumann, 1986: The relation between tropical cyclone motion and environmental geostrophic flows. *Mon. Wea. Rev.*, **114,** 115–122.

Dritschel, D. G., 1989: Contour dynamics and contour surgery: Numerical algorithms for extended, high resolution modelling of vortex dynamics in two-dimensional inviscid compressible flows. *Computer Phys. Rep.*, **10,** 77–146.

Elsberry, R. L., B. C. Diehl, J. C.-L. Chan, P. A. Harr, G. J. Holland, M. Lander, T. Neta, and D. Thom, 1990: ONR Tropical cyclone motion research initiative: Field experiment summary. Tech. Rep. NPS-MR-91-001, Naval Postgraduate School, Monterey, CA 94943, 107pp.

Evans, J. L., G. J. Holland, and R. L. Elsberry, 1991: Interactions between a barotropical vortex and an idealized subtropical ridge. Part I: Vortex motion. *J. Atmos. Sci.*, **48,** 301–314.

Fiorino, M., and R. L. Elsberry, 1989: Some aspects of vortex structure related to tropical cyclone motion. *J. Atmos. Sci.*, **46,** 975–990.

Franklin, J. L., 1990: Dropwindsonde observations of the environmental flow of Hurricane Josephine (1984): Relation to vortex motion. *Mon. Wea. Rev.*, **118,** 2732–2744.

George, J. E., and W. M. Gray, 1976: Tropical cyclone motion and surrounding parameter relationships. *J. Appl. Meteor.*, **15,** 1252–1264.

Holland, G. J., 1983: Tropical cyclone motion: Environmental interaction plus a beta effect. *J. Atmos. Sci.*, **40,** 328–342.

——, 1984: Tropical cyclone motion: A comparison of theory and observation. *J. Atmos. Sci.*, **41,** 68–75.

Hoskins, B. J., M. E. McIntyre, and A. W. Robertson, 1985: On the use and significance of isentropic potential-vorticity maps. *Quart. J. Roy. Meteor. Soc.*, **111,** 877–946.

Nielsen, J. W., C. A. Davis, and D. Keyser, 1991: Upper-level frontogenesis made easy? Preprint, *First Int. Winter Storm Symp.*, Amer. Meteor. Soc., 82–88.

Polvani, L. M., N. J. Zabusky, and G. R. Flierl, 1989: Two-layer geostrophic vortex dynamics. Part I. Upper layer V-states and merger. *J. Fluid: Mech.*, **205,** 215–242.

Rotunno, R., and K. A. Emanuel, 1987: An air–sea interaction theory for tropical cyclones: Part II. *J. Atmos. Sci.*, **44,** 542–561.

Shapiro, L. J., 1992: Hurricane vortex motion and evolution in a three-layer model. *J. Atmos. Sci.*, **49,** 140–153.

——, and K. V. Ooyama, 1990: Barotropic vortex evolution on a beta plane. *J. Atmos. Sci.*, **47,** 170–187.

Smith, R. K., W. Ulrich, and G. Dietachmayer, 1990: A numerical study of tropical cyclone motion using a barotropic model. I: The role of vortex asymmetries. *Quart. J. Roy. Meteor. Soc.*, **116,** 337–362.

Ulrich, W., and R. K. Smith, 1991: A numerical study of tropical cyclone motion using a barotropic model. II: Motion in spatially-varying large-scale flows. *Quart. J. Roy. Meteor. Soc.*, **117,** 107–124.